Title

Sequential Cascade Electrocatalytic Conversion of Carbon Dioxide to C-C Coupled Products

Journal

ACS Applied Energy Materials, 2(6)

ISSN

2574-0962

Authors

Gurudayal, G

Perone, D

Malani, S

et al.

Publication Date

2019-06-24

DOI

10.1021/acsaem.9b00791

Sequential Cascade Electrocatalytic Conversion of Carbon Dioxide to C-C Coupled Products

Gurudayal,[†,#,¶] *David Perone,*[Δ,†,‡,¶] *Saurabh Malani,* [£] *Yanwei Lum,*[†,‡,¶] *Sophia Haussener,*[Δ] *and Joel W. Ager*[*,†,‡,¶]

[†]Joint Center for Artificial Photosynthesis, [#]Chemical Sciences Division, and [‡]Materials Science Division, Lawrence Berkeley National Laboratory, California 94720, United States

[¶]Department of Materials Science and Engineering and [£]Department of Chemical Engineering and Biochemistry, University of California, Berkeley, California 94720, United States

[Δ]Department of Mechanical Engineering, École Polytechnique Fédéral de Lausanne, Lausanne 1015, Switzerland

AUTHOR INFORMATION

Corresponding Author

[*]To whom correspondence should be addressed: J.W. A. (email: jwager@lbl.gov)

KEYWORDS: Cascade catalysis, sequential catalysis, electrocatalysis, CO_2 reduction, renewable fuels,

ABSTRACT. Cascade catalytic processes perform multi-step chemical transformations without isolating the intermediates. Here, we demonstrate a sequential cascade pathway to convert CO_2 to C_{2+} hydrocarbons and oxygenates in a two-step electrocatalytic process using CO as the intermediate. CO_2 to CO conversion is performed by using Ag and further conversion of CO to C-C coupled products is performed with Cu. Temporal separation between the two reaction steps is accomplished by situating the Ag electrode upstream of the Cu electrode in a continuous flow reactor. Convection-diffusion simulations and experimental evaluation of the electrodes individually were performed to identify optimal conditions. With the upstream Ag electrode poised at -1 V vs RHE in a flow of CO_2-saturated water in aqueous carbonate buffer, over 80% of the CO can be converted on the downstream Cu electrode. When the Ag electrode is on, a supersaturation of CO is achieved near the Cu electrode, which leads to a relative increase in the formation rate of C_2 and C_3 oxygenates as compared to ethylene.

TOC GRAPHIC

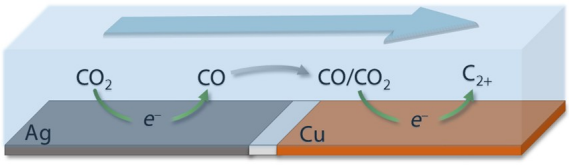

INTRODUCTION

In cascade catalysis two or more catalyzed reactions are coupled together in a single pot, without isolation of the reaction intermediates.[1,2] Natural photosynthesis provides a prototypical example of an enzymatic cascade,[3] and there has been intense interest in the prospects of coupling enzymes with synthetic homogeneous and heterogeneous catalysts to increase the reactivity, selectivity, and sustainability of chemical syntheses.[4–6] Cascade approaches using immobilized enzymes have also been used to increase the efficiency of methanol biofuel cells.[7]

In this context, developing approaches to convert CO_2 to chemicals and fuels using renewable power sources provides a grand challenge.[8,9] Indeed, multi-step conversion of CO_2 to methanol has been demonstrated using a sequence of metalorganic homogeneous catalysts under high temperature and pressure and by using a enzymes confined in micelles with NADH as the electron donor.[10,11] Recently, Somorjai, Yang and co-workers demonstrated thermal conversion of CO to C_2-C_4 hydrocarbons in a two-step cascade using CO as the reaction intermediate,[12] and Li and coworkers achieved selective production of aromatics using CH_xO species as intermediates.[13]

Electrochemical CO_2 reduction (CO_2R), which can be performed under mild conditions of ambient pressure and room temperature, is an excellent platform for exploring cascade approaches for selective chemical synthesis.[6,14] Following pioneering work by Hori and co-workers in the

1980s,[15] CO_2R has been the subject of intense recent interest, leading to an improved understanding of the possible products and the mechanisms for their formation.[16–25] Notably, catalysts (e.g. Ag, Au) which produce CO and which convert CO to C-C coupled products (e.g. Cu produced by oxidation/reduction cycling) have been identified.[26–33] Recently, a tandem CO_2 cascade was demonstrated using interdigitated Au and Cu electrodes; CO produced on the Au is able to diffuse over distances of 10's of microns where it undergoes further reaction on the Cu.[34] Interestingly, simulations of this system predict that the concentration of CO at the Cu electrode is well above its ca. 1 mM solubility limit; consistent with this prediction is the observation of a C_2 product distribution with a greatly increased ratio of oxygenates (ethanol, acetaldehyde, 1-propanol) compared to hydrocarbons (ethylene), with a similar trend being reported for CO reduction at elevated pressure.[27] It has also been predicted that a two-step CO_2 reduction cascade can lead to improved overall energetic conversion efficiencies.[35]

We hypothesized here that a related cascade process could be achieved using convection, as opposed to diffusion, to transport the intermediate. This approach (Scheme 1) represents a sequential tandem cascade in continuous flow,[5,36] with the temporal separation between the catalyst "compartments" being produced by directional flow of the electrolyte. In our prior work, with diffusional transport of the intermediate, the conversion efficiency is determined by the distance between the electrodes. With convective transport, the flow rate as well as the geometry controls the conversion rate,

which may allow for greater flexibility in design. It may also be possible to extend the approach by adding additional electrodes.

The approach is conceptually similar to the dual working electrode report of Kenkel and Bard, although in that case the electrodes were oppositely polarized, with one performing a reduction reaction and the other oxidation.[37] Recently, Spurgeon and co-workers have reported on a related, compartmentalized, approach for CO_2R, using Ag and Cu in separate chambers to, respectively, produce CO and to convert CO to ethanol.[38] However, well less than 10% of the intermediate CO was converted in the upstream chamber due to mixing during the transport between the chambers. In contrast, we will show that closer positioning of the electrodes reduces diffusion losses of the intermediate such that much higher conversion rates can be attained.

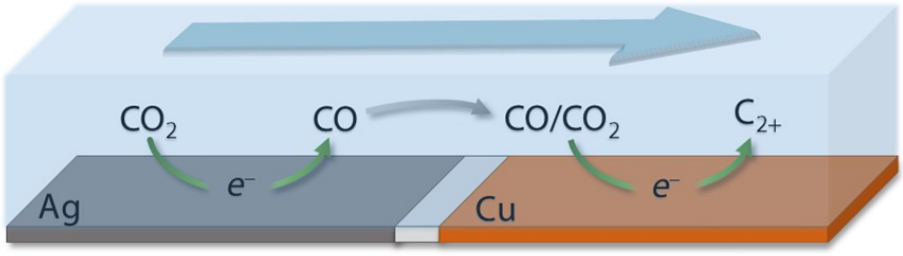

Scheme 1. Tandem cascade catalysis for reduction of CO_2 to C_{2+} products in a flow cell geometry. CO produced selectively by the upstream Ag electrode is further converted to C_2 products by the downstream Cu electrode. The potential on the two electrodes, as well as the flow rate through the reactor, can be independently tuned to maximize the conversion of the intermediate species.

RESULTS AND DISCUSSION

The overall cell design employed was based on our prior work showing that separation of product-containing catholyte and anolyte streams can be achieved by co-laminar flow.[39] The computational modeling approach of that study was extended to find conditions under which convectional transport of the CO intermediate to the downstream electrode could be efficient, in order to maximize its conversion, without encountering diffusion limitations associated with the supply of CO_2 to both electrodes. Independent control of the potential allowed for control of the supply of CO to the downstream electrode. Under optimized conditions, conversion efficiencies for the intermediates in the range of 40-80% are achieved. Operation in cascade mode, as compared to control experiments performed with only the Cu electrode activated, leads to an increase in the oxygenate to hydrocarbon ratio with the C-C coupled products.

Simulations. Simulations were performed to find operating conditions which would maximize the conversion of the intermediate while supplying sufficient amounts of reactants to both electrodes. A detailed description of the multiphysics modeling approach is in the SI; initial modeling with a similar flow system has been reported by Perone.[40] The model uses the equilibrium constants in the CO_2-bicarbonate-carbonate system to calculate the pH at the reactor entrance and uses the rate constants to calculate species concentrations in the reactor. Figure 1a shows the two dimensional simulation domain over which the corresponding transport and conservation

equations were solved so as to determine the velocity of the electrolyte, and the concentrations of CO, CO_2, HCO_3^-, CO_3^{2-}, and OH^- (pH) while considering the homogeneous bicarbonate and carbonate buffer chemistry.[41,42] A constant molar flux corresponding to a current density J_{Ag} was assumed at the Ag electrode; setting the CO concentration boundary condition to zero at the Cu cathode allows the diffusion limited conversion case to be considered. Volumetric flow rates Q between 1 and 20 cm^3 min^{-1} were evaluated; under these conditions calculated Reynolds numbers are far below typical values for turbulent flow (see SI). Entrance length effects were also evaluated but found to be minor.[40]

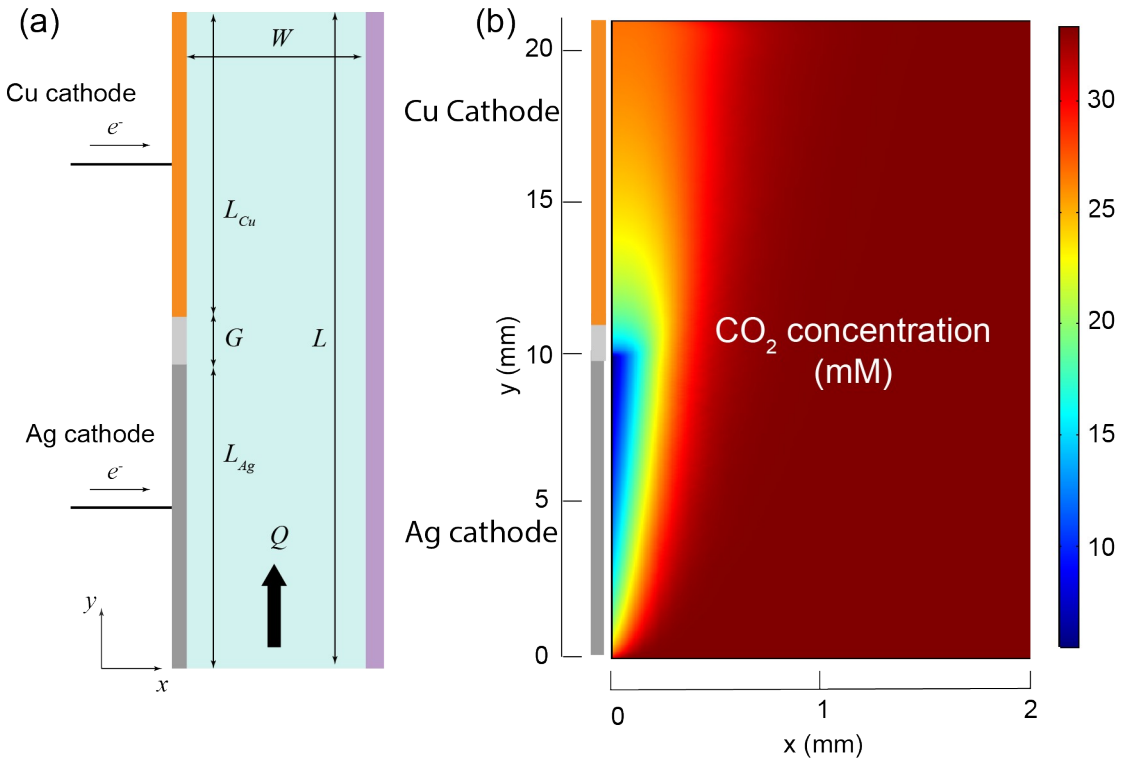

Figure 1. (a) Simulation domain with a flow Q of electrolyte in the cathode chamber. The right boundary of the domain is the anion conducting membrane used to separate the cathode chamber from the anode chamber.

The total length L of the chamber is 21 mm with a width W of 5 mm (height of chamber, not depicted, is 5 mm). The lengths L of the Ag and Cu electrodes are 10 mm with a 1 mm gap in between. (b) Calculated CO_2 concentration for Q = 2 cm^3 min^{-1} and J_{Ag} = 3 mA cm^{-2}. Note that for (b) only 40% of the full 5 mm width of the chamber is depicted.

First, simulations were performed to find operating conditions for the Ag electrode which would not completely deplete the CO_2 available to the downstream Cu electrode. Figure 1b shows the calculated CO_2 concentration for Q = 2 cm^3 min^{-1} and J_{Ag} = 3 mA cm^{-2} at the Ag electrode and for an inactive Cu electrode. Under these conditions, the minimum CO_2 concentration, 10 mM, is found at the downstream end of the Ag electrode (see SI for line graphs). The predicted maximum CO current density, achieved by completely depleting the CO_2 at the end of the Ag electrode, is 3.6 mA cm^{-2}. This limiting value can be increased, albeit sub-linearly, by increasing the flow rate. For example, a limiting Ag current density of 8.1 mA cm^{-2} is predicted for a flow rate of 20 cm^3 min^{-1}.

The maximum predicted conversion efficiency for the CO intermediate produced by the Ag electrode was evaluated by setting the CO concentration to zero at the Cu electrode. Figure 2 shows CO concentration contours and fluxes for inactive Cu (a and b) and with diffusion-limited conversion of CO at the Cu electrode (c and d). Comparison of the flux of CO leaving the reactor for the two cases allows the conversion efficiency to be predicted, which is 38% for this case (J_{Ag} = 3 mA cm^{-2}, Q = 2 cm^3 min^{-1}). The predicted

conversion efficiency decreases, again sub-linearly with increasing Q, with a value of 28% predicted for Q = 20 cm^3 min^{-1}. Notably, the predicted concentration of CO is very large, 22 mM at the end of the Ag electrode for the case considered in Figure 2. While these concentrations greatly exceed the equilibrium solubility of CO, ca. 1 mM, if bubbles do not nucleate, the simulation predicts that the CO activity near the Cu electrode can be increased far beyond what is possible with CO-saturated water as the electrolyte. Our prior work with interdigitated electrodes reached a similar conclusion.[34] As a result, we expect that the C_2 product distribution produced by the Cu under these CO-enhanced conditions will contain more oxygenates. On the other hand, the predicted pH near the Cu electrode is above 12 as shown in Figure S4. Recent work with gas diffusion electrode has shown that high pH favors ethylene production from CO and CO_2 reduction on Cu.[43,44]

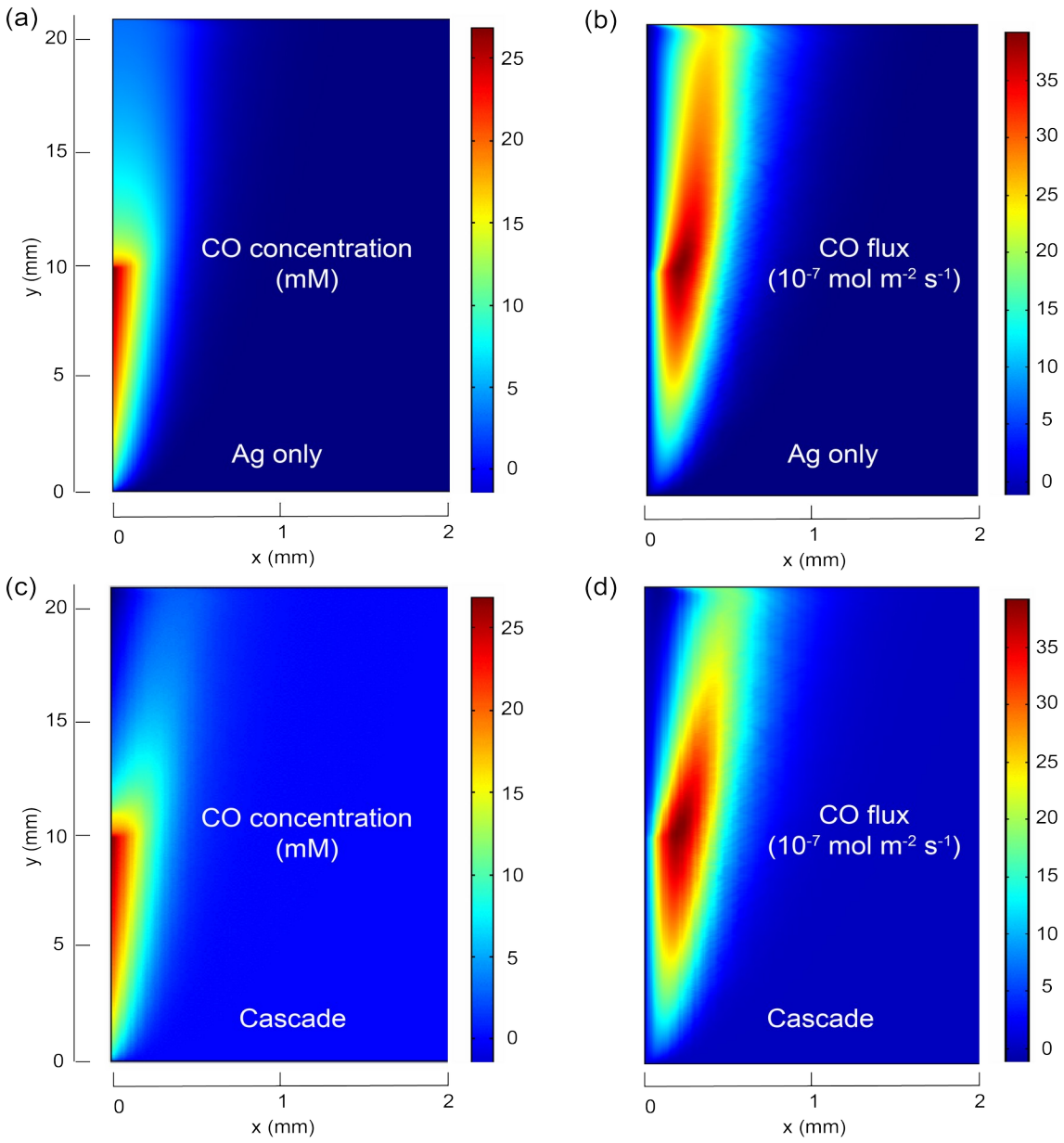

Figure 2. Contour plot of CO concentrations with a flow rate of 2 ml/min for a) an inactive Cu electrode and c) for cascade operation with diffusion-limited conversion at the Cu electrode. b) and d) Contour plots of CO flux (concentration * flow velocity) with Q = 2 cm^3 min^{-1}, current density for CO formation of 3 mA cm^{-2} at the Ag electrode for b) an inactive Cu electrode

and d) for cascade operation with diffusion-limited conversion at the Cu electrode.

Experimental electrolysis cell. Figure 3 depicts the flow cell used in the experimental work. 0.1 M $CsHCO_3$ electrolyte saturated with CO_2 (ca. 33 mM) was used as the electrolyte in both the cathode and anode chambers and was circulated by peristaltic pumps. A nanostructured IrO_2 anode was used to drive the oxygen evolution reaction in the anode chamber.[45] We found it beneficial for sustained operation to employ an ion exchange resin (Chelex®) to getter metals from the anode which would otherwise deposit on the cathodes and increase the rate of the competing hydrogen evolution reaction.[46] An anion exchange membrane (SELEMION™) was used to separate the cathode and anode chambers. We performed initial experiments without the anion exchange membrane but encountered difficulties with cross-contamination of metals from the anode and also oxidation of the products. The Ag and Cu cathodes were operated independently in bipotenstiostatic mode with respect to a common reference electrode in the cathode chamber (see Method section in SI for details). Gas products were evaluated by sampling the gas exiting the saturation volume on the cathode side. Liquid products were evaluated by HPLC at the end of a run (see SI for details). In cascade operation, the sum of currents from the electrodes is used in the calculation of the faradaic efficiencies (FEs) of the gaseous products, and the total charge passing into the cell through both

electrodes is used to calculate the FE of liquid products. A detailed discussion of FE calculation of gaseous and liquid products is in the SI.

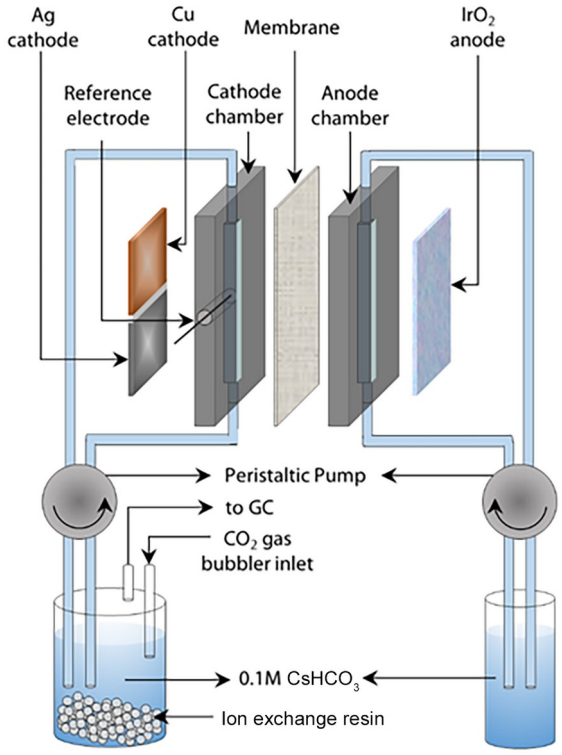

Figure 3. Schematic of flow reactor used for cascade electrocatalytic reduction of CO_2.

Optimization of the CO intermediate production. The Ag electrode was operated by itself to find conditions which would provide a well-defined supply of the cascade intermediate to the Cu electrode, the second step in the cascade. As suggested by the modeling, a flow rate of 2 cm^3 min^{-1} was used for these experiments and for all subsequent experiments discussed here. Results of varying the potential on the Ag between -0.6 and -1.2 vs. RHE with the Cu electrode deactivated are shown in Figure 4a. The only two products observed are CO and H_2 and the sum of their faradaic efficiencies

(FEs) is 100% within experimental error, which provides an internal validation of our analytical methods. The maximum FE to CO, the desired intermediate product, is ca. 90% at a potential of -1.0 V vs RHE. The total current density for this electrode at that potential is 6.4 mA cm^{-2}. At larger overpotentials, the FE for H_2 increases, which is likely due to the mass transfer limit for the CO_2 supply predicted by the simulations. We note that the current density for CO production at -1.0 and -1.2 vs RHE exceeds by about a factor of two the diffusion limit predicted by our simulations. We do not know the reason for this effect but do note that there are reports in the literature of CO_2 reduction current densities in stirred reactors (e.g. 40 mA cm^{-2} for C_{2+} product production from nanostructured Cu from Jiang *et al*.[47]) which exceed the predictions of 1D modeling by a similar factor.[41]

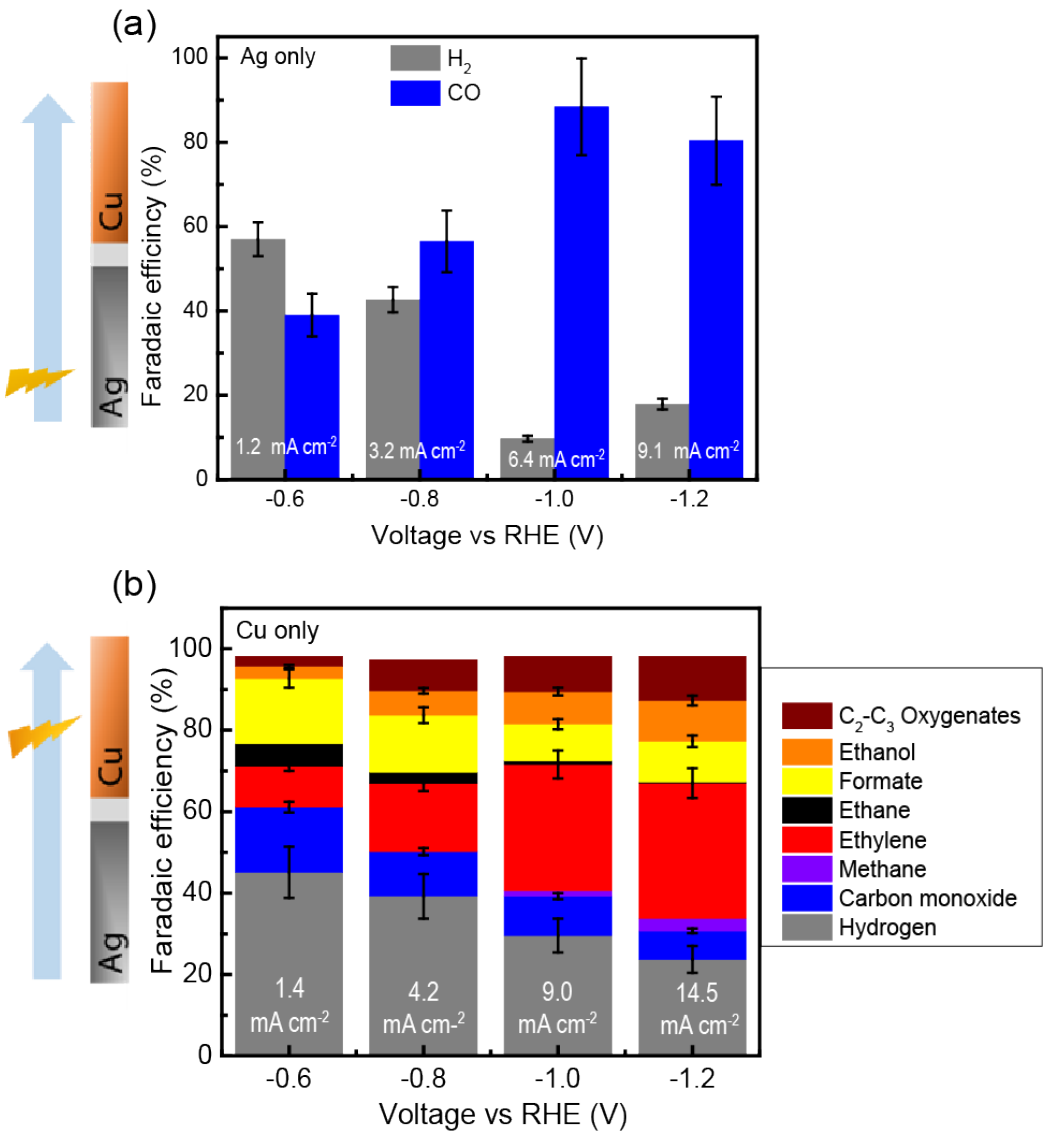

Figure 4. Faradaic efficiency as a function of potential applied to a) the Ag cathode (Cu inactive), and b) the Cu cathode (Ag inactive), both performed in a recirculating flow (2 ml/min) of 0.1 M $CsHCO_3$ electrolyte saturated with CO_2. Error bars are standard deviations from repeat experiments, minimum 3.

Optimization of the second step of cascade. The Cu electrode was operated by itself to assess its activity for the CO_2 reduction, which will occur concurrently with reduction of CO provided by the Ag cathode when the

reactor is operated in cascade mode. Results of varying the potential on the Cu between -0.6 and -1.2 vs. RHE with the Ag electrode deactivated are shown in Figure 4b. Major products observed are H_2, CO, C_2H_4, formate, ethanol, and other C_{2+} oxygenates such as 1-propanol, allyl alcohol, acetaldehyde and propionaldehyde (see SI for full product analysis details). The FE for H_2 decreases with increasing overpotential as does the FE for CO. As with the Ag optimization experiments, the FEs sum to 100% within experimental error. The FEs are very similar to what we have reported before for similarly synthesized Cu evaluated in a more typical sandwich cell under the same electrolyte conditions.[48]

Operation in cascade catalysis mode. Sequential cascade electrocatalysis is accomplished by fixing the Ag electrode at its maximum CO selectivity (-1.0 V vs RHE) and varying the potential of the Cu electrode. In principle, it would be possible to operate the Ag electrode at more negative potentials to further increase the CO flux. However, this would lead to an decrease in the CO_2 reduction selectivity as the additional H_2 would not be converted on the Cu electrode. Figure 5a shows the current density at the Cu electrode as a function of potential for Cu-only and cascade modes. At lower overpotentials, the current density is higher in cascade mode. This is an expected result, as CO reduction has a lower overpotential on Cu compared to CO_2 reduction.[27] Although there is some overlap in error bars, a possible trend can be seen in the current density on the Cu in cascade vs Cu-only mode as the overpotential on the Cu electrode is increased. The current

density of Cu electrode in cascade mode is slightly higher at lower overpotentials, -0.6 V and -0.8 V vs RHE, but crosses over and becomes lower at larger potentials. This observation could be rationalized by considering the number of electrons needed to make COR and CO_2R products. Specifically, CO reduction requires two fewer electrons compared to CO_2 on a per carbon basis for a given product. Thus, the crossover in the Cu current density reflects the increasing contribution of CO_2 reduction as the driving force is increased.

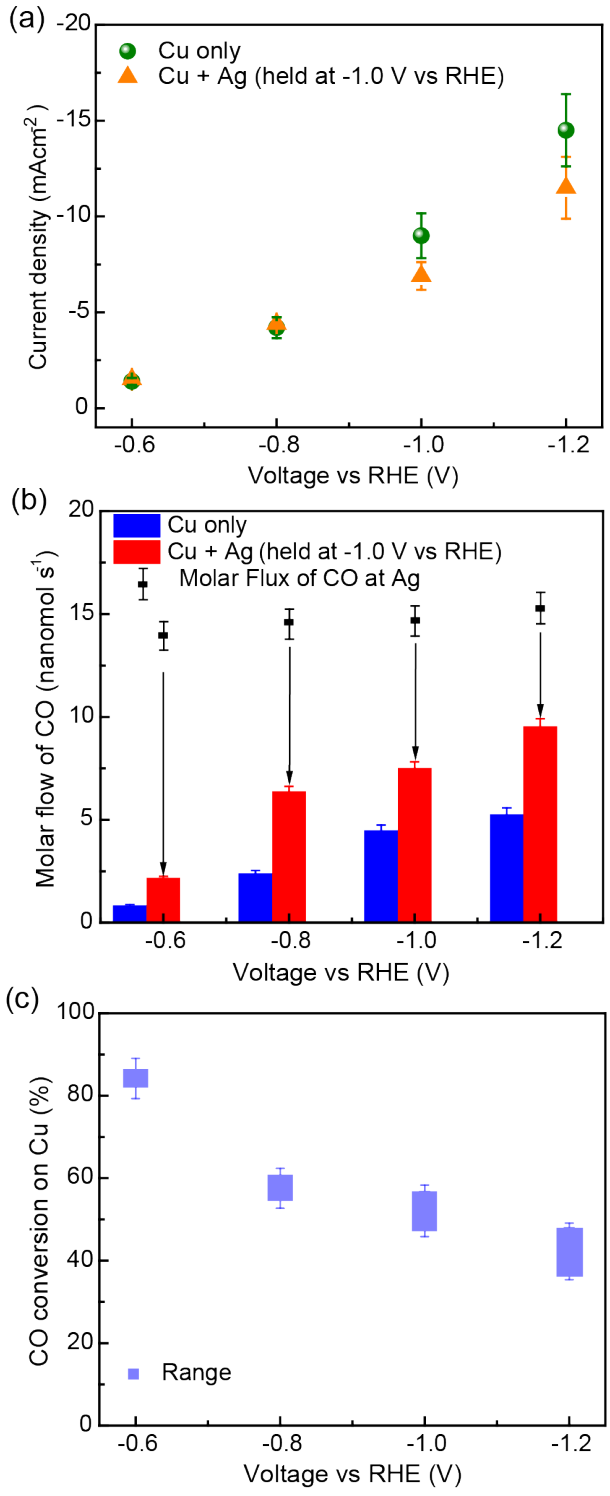

Figure 5. (a) Average current density of Cu only (green circles) and under cascade operation (orange triangles) as a function of the potential applied to

the Cu, -0.6 V vs RHE to -1.2 V vs RHE. (b) Molar flow to CO of only the Ag electrode (black squares), only the Cu electrode (blue bar) and under cascade operation (red bar), as a function of potential applied to the Cu electrode. The arrow shows the reduction in overall CO flux in cascade operation as compared to Ag only mode. (c) Range for conversion efficiency of the CO intermediate on the Cu electrode in cascade mode as a function of potential (see text). The Ag electrode was held at -1.0 V vs RHE in cascade operation.

The molar flow of CO in Ag only, Cu only and cascade mode was derived from -0.6 V to -1.2 V vs RHE by dividing the partial currents to CO by the Faraday constant (Figure 5b). The two electrodes are not completely independent, and a slight increase in the current of the Ag electrode was observed as the overpotential on the Cu electrode was increased. To compute the molar flux of CO from the Ag in cascade mode, black squares in Figure 5b, it was assumed that the FE remains at 90%. The arrows in Figure 5b show clearly the suppression of CO molar flow in cascade operation at all voltages, which means a large fraction of CO generated by the Ag electrode is consumed by copper.

In order to evaluate the CO conversion efficiency, we determined the upper and lower limits as follows (detailed discussion is presented in Supplemental Materials). We assume that the molar CO flow from the Ag is the same in cascade mode as it is in Ag-only mode. To determine the upper limit of the conversion efficiency, we assume that the CO molar flow from Cu is the same

in cascade mode as it is in only Cu mode. In this case, the conversion efficiency is determined by taking the sum of the CO molar flows in Ag-only and Cu-only modes, subtracting the CO molar flow in cascade mode, and dividing by the sum of the CO fluxes in Ag-only and Cu-only modes. To determine the lower limit, we consider that CO production from CO_2 reduction on Cu could be shut off in cascade mode. This could happen if direct adsorption of CO from the upstream electrode outcompetes CO_2 reduction for active sites on the Cu. In this case, the conversion efficiency is simply determined subtracting the CO molar flow in cascade mode from the Ag-only molar flow and dividing by the Ag-only molar flow. As the actual situation may fall between these two cases, we show the conversion efficiency as a range in Figure 5c. The CO conversion efficiency is high (over 50% and as high as 84%) at lower voltages (i.e., -0.6 and -0.8 V vs RHE on the Cu). We attribute the high conversion efficiency to the lower overpotential required for COR vs CO_2R on Cu. At higher potentials on the Cu, the conversion efficiency drops (but still is higher than 37%) as direct CO_2 reduction on Cu starts to outcompete diffusion-limited CO reduction.

Effect of cascade catalysis on product distribution. CO_2RR product distribution in cascade operation is shown in Figure 6a. The FE for H_2 decreases with increasing potential, similar to the Cu-only operation (Figure 4b). The decreasing FE for CO as a function of potential reflects the efficiency of the intermediate conversion and the relative increase of direct CO_2 conversion on Cu as discussed above. Strikingly, the oxygenate to ethylene

ratio (Figure 6b) is increased in cascade mode with a maximum of 1.95 at -0.8 V vs RHE. This observation is similar to the prior report with a diffusional cascade and to observations of CO reduction at elevated pressure, although the precise mechanism for this effect is not yet clear.[27, 34,49] It is also notable that the FE for H_2 is lower in cascade mode compared to Cu-only and is less than 20% with the Cu electrode held at -1.2 V vs. RHE. Operation of the Cu electrode at higher voltage (-1.4 V vs RHE) led to an increased FE for H_2, which we attribute to reaching diffusion limitations for the CO_2 (Figure S6b). Operating the Cu at lower voltage, -0.4 V vs RHE, also led to an increase in FE for H_2, reflective of an overall decrease in FE for COR with this small driving force (Figure. S6a).

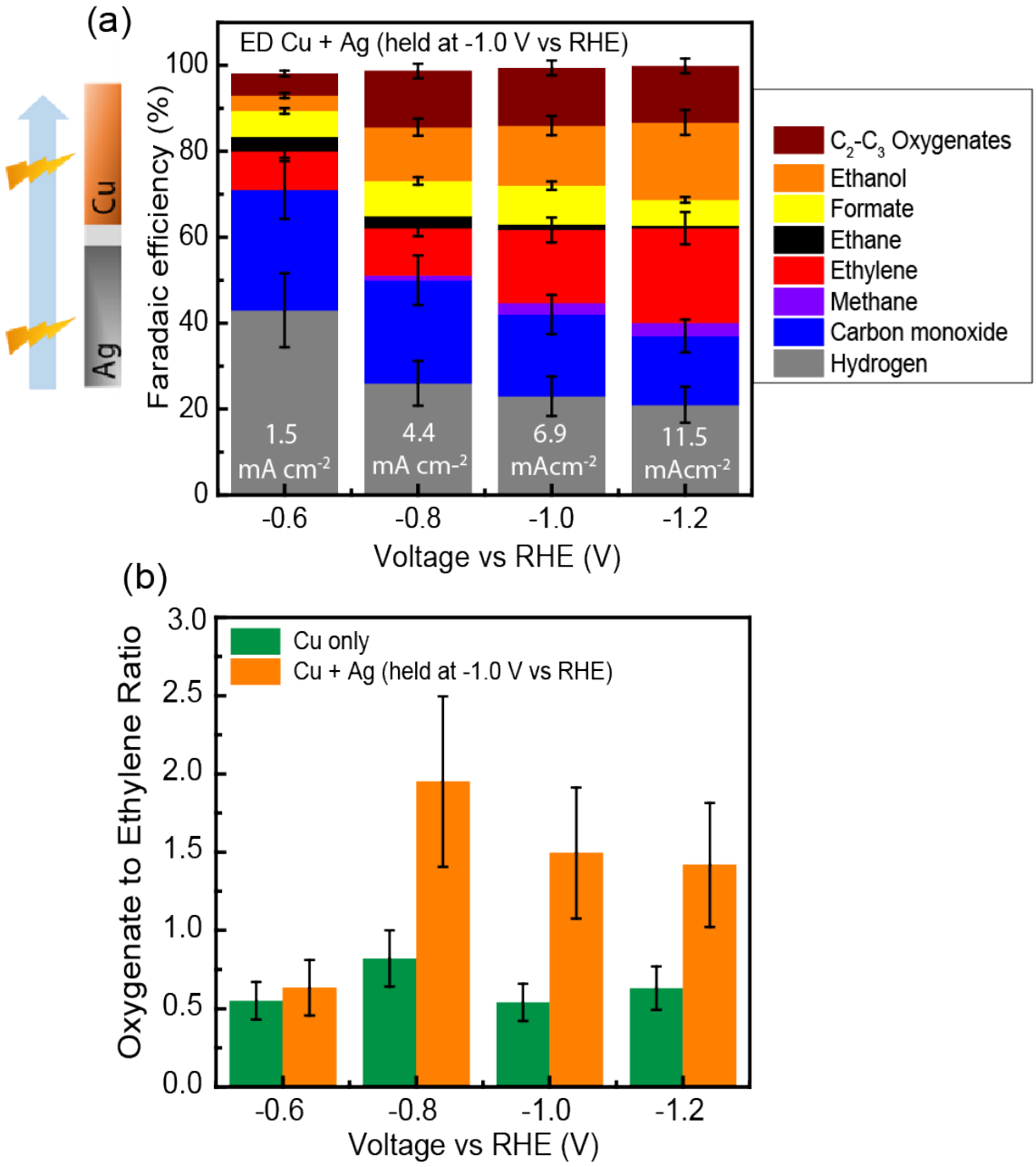

Figure 6. (a) Product distribution in cascade operation. The current density on the Cu is indicated on the solid bars. (b) Oxygenate to ethylene ratio as a function of voltage in cascade mode. Error bars are standard deviations from repeat experiments, minimum 3.

CO reduction. To provide further evidence of CO supersaturation near the Cu electrode in cascade mode, as predicted by the simulations (Figure 1b), control experiments were performed with a flow of CO saturated 0.05 M Cs_2CO_3 (pH 11.95) electrolyte for CO reduction in the flow cell with only the Cu activated. At the potentials at which we observed an enhanced oxygenates to ethylene ratio in cascade mode, -0.6 to -1.0 V vs. RHE, the ratio observed for CO reduction was lower (Figure S7). As it is known that increased CO concentration favors oxygenate production[16,49–51], we take this as evidence of a supersaturated CO condition in cascade mode.

Investigation of bubble nucleation. The simulations predict CO concentrations near the Ag electrode far in excess of its ca. 1 mM equilibrium solubility at 1 atm pressure. If bubbles were to nucleate, we would expect two effects: (1) bubbles could block the surface cites of the cathode and reduce the current density and (2) less CO would be available via convective transfer to the downstream Cu cathode. On the other hand, it is known from work with HER, which similarly generates an insoluble product, that it is possible to reach high supersaturations, particularly if the electrode surface is smooth.[52–54] To qualitatively evaluate bubble formation, we replaced the opaque IrO_2 electrode with a Pt wire such that the surfaces of the Cu and Ag electrodes became visible (supplementary movie). Next, we operated this configuration in cascade mode (Ag at -1.0 V vs RHE and Cu at -1.2 V vs RHE). The Pt wire efficiently nucleates oxygen bubbles, and thus serves as a qualitative reference of the product formation rate. Compared to the Pt wire,

only a very few, small, bubbles were generated from the Ag cathode. We conclude that at the current densities used bubble formation does not significantly affect intermediate transport to the downstream electrode.

CONCLUSIONS

Sequential cascade CO_2 reduction has been demonstrated by electrocatalysis using two working electrodes (Ag and Cu). The CO intermediate produced by Ag is transported by convective flow to the Cu for further conversion. A computational analysis was performed to identify the ideal operating conditions to confirm the optimum transport of CO from Ag to Cu via convection and diffusion. Experimentally, we find that the intermediate conversion can be over 80% and was over ~40% for the current and electrolyte flow conditions employed in the study. The upstream Ag cathode produces a supersaturated CO concentration at the downstream Cu electrode, which increase the production of C-C coupled oxygenate products. A maximum in the oxygenate to ethylene ratio is obtained by operation the Ag electrode at -1 V vs RHE with the Cu electrode at -0.8 vs RHE. It is conceptually possible to scale the approach to more electrodes and different geometries and to, potentially, couple it to enzymatic processes as proposed by Nam and co-workers.[14]

ASSOCIATED CONTENT

Supporting Information. Simulation methods and supplemental modeling results, experimental methods, supplementary electrochemical data, calculation of conversion efficiency, movie of cascade cell operation. This material is available free of charge via the Internet at http://pubs.acs.org.

Author Contributions

The manuscript was written through contributions of all authors. All authors have given approval to the final version of the manuscript. DP, G, SH, and JA conceived the experiment. DP performed initial simulation, cell fabrication, and electrochemical measurements. SM and YL performed supporting simulations to optimize the cell design. G designed and fabricated cells, performed electrochemical measurements, and product analyses.

Notes

The authors declare no competing financial interests.

ACKNOWLEDGMENT

This material is based upon work performed by the Joint Center for Artificial Photosynthesis, a DOE Energy Innovation Hub, supported through the Office of Science of the U.S. Department of Energy under Award Number DE-SC0004993. This material is also based upon work performed with the financial support of a Starting Grant of the Swiss National Science Foundation, as part of the SCOUTS project (grant #155876). We would like to thank Dr. Rob Roberts and Dr. Jaroslaw Syzdek from Bio-Logic for help in

developing the bipotentiostatic measurement mode. We thank the Molecular Graphics and Computation Facility, College of Chemistry, University of California Berkeley, supported by the National Science Foundation, grant CHE-08040, and by the National Institutes of Health, grant S10OD023532, for providing access to computing resources.

REFERENCES

(1) Bruggink, A.; Schoevaart, R.; Kieboom, T. Concepts of Nature in Organic Synthesis: Cascade Catalysis and Multistep Conversions in Concert. *Org. Process Res. Dev.* **2003**, *7*, 622–640.

(2) Kroutil, W.; Rueping, M. Introduction to ACS Catalysis Virtual Special Issue on Cascade Catalysis. *ACS Catal.* **2014**, *4*, 2086–2087.

(3) Shi, J.; Jiang, Y.; Jiang, Z.; Wang, X.; Wang, X.; Zhang, S.; Han, P.; Yang, C. Enzymatic Conversion of Carbon Dioxide. *Chem. Soc. Rev.* **2015**, *44*, 5981–6000.

(4) Grondal, C.; Jeanty, M.; Enders, D. Organocatalytic Cascade Reactions as a New Tool in Total Synthesis. *Nat. Chem.* **2010**, *2*, 167–178.

(5) Rudroff, F.; Mihovilovic, M. D.; Gröger, H.; Snajdrova, R.; Iding, H.; Bornscheuer, U. T. Opportunities and Challenges for Combining Chemo- and Biocatalysis. *Nat. Catal.* **2018**, *1*, 12–22.

(6) Ye, R.; Zhao, J.; Wickemeyer, B. B.; Toste, F. D.; Somorjai, G. A. Foundations and Strategies of the Construction of Hybrid Catalysts for Optimized Performances. *Nat. Catal.* **2018**, *1*, 318–325.

(7) Xia, L.; Van Nguyen, K.; Holade, Y.; Han, H.; Dooley, K.; Atanassov, P.; Banta, S.; Minteer, S. D. Improving the Performance of Methanol Biofuel Cells Utilizing an Enzyme Cascade Bioanode with DNA-Bridged Substrate Channeling. *ACS Energy Lett.* **2017**, *2*, 1435–1438.

(8) Graves, C.; Ebbesen, S. D.; Mogensen, M.; Lackner, K. S. Sustainable Hydrocarbon Fuels by Recycling CO_2 and H2O with Renewable or Nuclear Energy. *Renew. Sustain. Energy Rev.* **2011**, *15*, 1–23.

(9) Chu, S.; Majumdar, A. Opportunities and Challenges for a Sustainable Energy Future. *Nature* **2012**, *488*, 294–303.

(10) Huff, C. A.; Sanford, M. S. Cascade Catalysis for the Homogeneous Hydrogenation of CO 2 to Methanol. *J. Am. Chem. Soc.* **2011**, *133*, 18122–18125.

(11) Wang, X.; Li, Z.; Shi, J.; Wu, H.; Jiang, Z.; Zhang, W.; Song, X.; Ai, Q. Bioinspired Approach to Multienzyme Cascade System Construction for Efficient Carbon Dioxide Reduction. *ACS Catal.* **2014**, *4*, 962–972.

(12) Xie, C.; Chen, C.; Yu, Y.; Su, J.; Li, Y.; Somorjai, G. A.; Yang, P. Tandem Catalysis for CO 2 Hydrogenation to C 2 –C 4 Hydrocarbons. *Nano Lett.* **2017**, *17*, 3798–3802.

(13) Li, Z.; Qu, Y.; Wang, J.; Liu, H.; Li, M.; Miao, S.; Li, C. Highly Selective Conversion of Carbon Dioxide to Aromatics over Tandem Catalysts. *Joule* **2019**, *3*, 570–583.

(14) Yang, K. D.; Lee, C. W.; Jin, K.; Im, S. W.; Nam, K. T. Current Status and Bioinspired Perspective of Electrochemical Conversion of CO 2 to a Long-Chain Hydrocarbon. *J. Phys. Chem. Lett.* **2017**, *8*, 538–545.

(15) Hori, Y. Electrochemical CO2 Reduction on Metal Electrodes. In *Modern Aspects of Electrochemistry*; Vayenas, C. G., White, R. E., Gamboa-Aldeco, M. E., Eds.; Modern Aspects of Electrochemistry; Springer New York: New York, NY, 2008; pp 89–189.

(16) Peterson, A. A.; Abild-Pedersen, F.; Studt, F.; Rossmeisl, J.; Nørskov, J. K.; Norskov, J. K. How Copper Catalyzes the Electroreduction of Carbon Dioxide into Hydrocarbon Fuels. *Energy Environ. Sci.* **2010**, *3*, 1311.

(17) Kuhl, K. P.; Cave, E. R.; Abram, D. N.; Jaramillo, T. F. New Insights into the Electrochemical Reduction of Carbon Dioxide on Metallic Copper Surfaces. *Energy Environ. Sci.* **2012**, *5*, 7050.

(18) Costentin, C.; Robert, M.; Savéant, J.-M. Catalysis of the Electrochemical Reduction of Carbon Dioxide. *Chem. Soc. Rev.* **2013**, *42*, 2423–2436.

(19) Jones, J.-P.; Prakash, G. K. S.; Olah, G. A. Electrochemical CO 2 Reduction: Recent Advances and Current Trends. *Isr. J. Chem.* **2014**, *54*, 1451–1466.

(20) Qiao, J.; Liu, Y.; Hong, F.; Zhang, J. A Review of Catalysts for the Electroreduction of Carbon Dioxide to Produce Low-Carbon Fuels. *Chem. Soc. Rev.* **2014**, *43*, 631–675.

(21) Kortlever, R.; Shen, J.; Schouten, K. J. P.; Calle-Vallejo, F.; Koper, M. T. M. Catalysts and Reaction Pathways for the Electrochemical Reduction of Carbon Dioxide. *J. Phys. Chem. Lett.* **2015**, *6*, 4073–4082.

(22) Lu, Q.; Rosen, J.; Jiao, F. Nanostructured Metallic Electrocatalysts for Carbon Dioxide Reduction. *ChemCatChem* **2015**, *7*, 38–47.

(23) Kumar, B.; Brian, J. P.; Atla, V.; Kumari, S.; Bertram, K. A.; White, R. T.; Spurgeon, J. M. New Trends in the Development of Heterogeneous Catalysts for Electrochemical CO 2 Reduction. *Catal. Today* **2016**, *270*, 19–30.

(24) Montoya, J. H.; Seitz, L. C.; Chakthranont, P.; Vojvodic, A.; Jaramillo, T. F.; Nørskov, J. K. Materials for Solar Fuels and Chemicals. *Nat. Mater.* **2016**, *16*, 70–81.

(25) Mistry, H.; Varela, A. S.; Kühl, S.; Strasser, P.; Cuenya, B. R. Nanostructured Electrocatalysts with Tunable Activity and Selectivity. *Nat. Rev. Mater.* **2016**, *1*, 16009.

(26) Chen, Y.; Li, C. W.; Kanan, M. W. Aqueous CO 2 Reduction at Very Low Overpotential on Oxide-Derived Au Nanoparticles. *J. Am. Chem. Soc.* **2012**, *134*, 19969–19972.

(27) Li, C. W.; Ciston, J.; Kanan, M. W. Electroreduction of Carbon Monoxide to Liquid Fuel on Oxide-Derived Nanocrystalline Copper. *Nature* **2014**, *508*, 504–507.

(28) Verdaguer-Casadevall, A.; Li, C. W.; Johansson, T. P.; Scott, S. B.; McKeown, J. T.; Kumar, M.; Stephens, I. E. L.; Kanan, M. W.; Chorkendorff, I. Probing the Active Surface Sites for CO Reduction on Oxide-Derived Copper Electrocatalysts. *J. Am. Chem. Soc.* **2015**, *137*, 9808–9811.

(29) Jee, M. S.; Jeon, H. S.; Kim, C.; Lee, H.; Koh, J. H.; Cho, J.; Min, B. K.; Hwang, Y. J. Enhancement in Carbon Dioxide Activity and Stability on Nanostructured Silver Electrode and the Role of Oxygen. *Appl. Catal. B Environ.* **2016**, *180*, 372–378.

(30) Ma, M.; Trześniewski, B. J.; Xie, J.; Smith, W. A. Selective and Efficient Reduction of Carbon Dioxide to Carbon Monoxide on Oxide-Derived Nanostructured Silver Electrocatalysts. *Angew. Chemie Int. Ed.* **2016**, *55*, 9748–9752.

(31) Kim, C.; Jeon, H. S.; Eom, T.; Jee, M. S.; Kim, H.; Friend, C. M.; Min, B. K.; Hwang, Y. J. Achieving Selective and Efficient Electrocatalytic Activity for CO 2 Reduction Using Immobilized Silver Nanoparticles. *J. Am. Chem. Soc.* **2015**, *137*, 13844–13850.

(32) Rosen, B. A.; Salehi-Khojin, A.; Thorson, M. R.; Zhu, W.; Whipple, D. T.; Kenis, P. J. A.; Masel, R. I. Ionic Liquid-Mediated Selective Conversion of CO2 to CO at Low Overpotentials. *Science* **2011**, *334*, 643–644.

(33) Kumar, B.; Asadi, M.; Pisasale, D.; Sinha-Ray, S.; Rosen, B. A.; Haasch, R.; Abiade, J.; Yarin, A. L.; Salehi-Khojin, A. Renewable and Metal-Free Carbon Nanofibre Catalysts for Carbon Dioxide Reduction. *Nat. Commun.* **2013**, *4*, 2819.

(34) Lum, Y.; Ager, J. W. Sequential Catalysis Controls Selectivity in Electrochemical CO 2 Reduction on Cu. *Energy Environ. Sci.* **2018**, *11*, 2935–2944.

(35) Zhou, X.; Xiang, C. Comparative Analysis of Solar-to-Fuel Conversion

Efficiency: A Direct, One-Step Electrochemical CO 2 Reduction Reactor versus a Two-Step, Cascade Electrochemical CO 2 Reduction Reactor. *ACS Energy Lett.* **2018**, *3*, 1892–1897.

(36) Yuryev, R.; Strompen, S.; Liese, A. Coupled Chemo(Enzymatic) Reactions in Continuous Flow. *Beilstein J. Org. Chem.* **2011**, *7*, 1449–1467.

(37) Kenkel, J. V; Bard, A. J. A Dual Working Electrode Coulometric Flow Cell. *J. Electroanal. Chem. Interfacial Electrochem.* **1974**, *54*, 47–54.

(38) Theaker, N.; Strain, J. M.; Kumar, B.; Brian, J. P.; Kumari, S.; Spurgeon, J. M. Heterogeneously Catalyzed Two-Step Cascade Electrochemical Reduction of CO 2 to Ethanol. *Electrochim. Acta* **2018**, *274*, 1–8.

(39) Monroe, M. M.; Lobaccaro, P.; Lum, Y.; Ager, J. W. Membraneless Laminar Flow Cell for Electrocatalytic CO 2 Reduction with Liquid Product Separation. *J. Phys. D. Appl. Phys.* **2017**, *50*, 154006.

(40) Perone, D. Membraneless Laminar Flow Cell Using Sequential Catalysis for Electrochemical CO2 Conversion, École Polytechnique Fédérale de Lausanne, 2017.

(41) Gupta, N.; Gattrell, M.; MacDougall, B. Calculation for the Cathode Surface Concentrations in the Electrochemical Reduction of CO2 in KHCO3 Solutions. *J. Appl. Electrochem.* **2006**, *36*, 161–172.

(42) Singh, M. R.; Clark, E. L.; Bell, A. T. Effects of Electrolyte, Catalyst, and Membrane Composition and Operating Conditions on the Performance of Solar-Driven Electrochemical Reduction of Carbon Dioxide. *Phys. Chem. Chem. Phys.* **2015**, *17*, 18924–18936.

(43) Dinh, C.-T.; Burdyny, T.; Kibria, M. G.; Seifitokaldani, A.; Gabardo, C. M.; García de Arquer, F. P.; Kiani, A.; Edwards, J. P.; De Luna, P.; Bushuyev, O. S.; Zou, C.; Quintero-Bermudez, R.; Pang, Y.; Sinton, D.; Sargent, E. H. CO 2 Electroreduction to Ethylene via Hydroxide-Mediated Copper Catalysis at an Abrupt Interface. *Science* **2018**, *360*, 783–787.

(44) Han, L.; Zhou, W.; Xiang, C. High-Rate Electrochemical Reduction of Carbon Monoxide to Ethylene Using Cu-Nanoparticle-Based Gas Diffusion Electrodes. *ACS Energy Lett.* **2018**, *3*, 855–860.

(45) Gurudayal; Bullock, J.; Srankó, D. F.; Towle, C. M.; Lum, Y.; Hettick, M.; Scott, M. C.; Javey, A.; Ager, J. W. Efficient Solar-Driven Electrochemical CO 2 Reduction to Hydrocarbons and Oxygenates. *Energy Environ. Sci.* **2017**, *10*, 2222–2230.

(46) Ren, D.; Loo, N. W. X.; Gong, L.; Yeo, B. S. Continuous Production of Ethylene from Carbon Dioxide and Water Using Intermittent Sunlight. *ACS Sustain. Chem. Eng.* **2017**, *5*, 9191–9199.

(47) Jiang, K.; Sandberg, R. B.; Akey, A. J.; Liu, X.; Bell, D. C.; Nørskov, J. K.;

Chan, K.; Wang, H. Metal Ion Cycling of Cu Foil for Selective C–C Coupling in Electrochemical CO2 Reduction. *Nat. Catal.* **2018**, *1*, 111–119.

(48) Lum, Y.; Yue, B.; Lobaccaro, P.; Bell, A. T.; Ager, J. W. Optimizing C–C Coupling on Oxide-Derived Copper Catalysts for Electrochemical CO 2 Reduction. *J. Phys. Chem. C* **2017**, *121*, 14191–14203.

(49) Wang, L.; Nitopi, S. A.; Bertheussen, E.; Orazov, M.; Morales-Guio, C. G.; Liu, X.; Higgins, D. C.; Chan, K.; Nørskov, J. K.; Hahn, C.; Jaramillo, T. F. Electrochemical Carbon Monoxide Reduction on Polycrystalline Copper: Effects of Potential, Pressure, and PH on Selectivity toward Multicarbon and Oxygenated Products. *ACS Catal.* **2018**, *8*, 7445–7454.

(50) Xiao, H.; Cheng, T.; Goddard, W. A.; Sundararaman, R. Mechanistic Explanation of the PH Dependence and Onset Potentials for Hydrocarbon Products from Electrochemical Reduction of CO on Cu (111). *J. Am. Chem. Soc.* **2016**, *138*, 483–486.

(51) Calle-Vallejo, F.; Koper, M. T. M. Theoretical Considerations on the Electroreduction of CO to C2Species on Cu(100) Electrodes. *Angew. Chemie - Int. Ed.* **2013**, *52*, 7282–7285.

(52) Vogt, H.; Balzer, R. J. The Bubble Coverage of Gas-Evolving Electrodes in Stagnant Electrolytes. *Electrochim. Acta* **2005**, *50*, 2073–2079.

(53) Bowers, P. G.; Hofstetter, C.; Letter, C. R.; Toomey, R. T. Supersaturation Limit for Homogeneous Nucleation of Oxygen Bubbles in Water at Elevated Pressure: “Super-Henry’s Law.” *J. Phys. Chem.* **1995**, *99*, 9632–9637.

(54) Matsushima, H.; Kiuchi, D.; Fukunaka, Y. Measurement of Dissolved Hydrogen Supersaturation during Water Electrolysis in a Magnetic Field. *Electrochim. Acta* **2009**, *54*, 5858–5862.